Accepted in ApJ, 2007 December 2
Preprint typeset using LaTeX style emulateapj v. 10/09/06

X-RAY AND NEAR-IR VARIABILITY OF THE ANOMALOUS X-RAY PULSAR 1E 1048.1−5937: FROM QUIESCENCE BACK TO ACTIVITY

Cindy R. Tam,[1] Fotis P. Gavriil,[2,3] Rim Dib,[1] Victoria M. Kaspi,[1,4] Peter M. Woods, [5,6] Cees Bassa,[1]

Accepted in ApJ, 2007 December 2

ABSTRACT

We report on new and archival X-ray and near-infrared (near-IR) observations of the anomalous X-ray pulsar 1E 1048.1−5937 performed between 2001-2007 with the *Rossi X-ray Timing Explorer* (*RXTE*), the *Chandra X-ray Observatory* (*CXO*), the *Swift Gamma-ray Burst Explorer*, the *Hubble Space Telescope* (*HST*), and the *Very Large Telescope*. During its ∼2001-2004 active period, 1E 1048.1−5937 exhibited two large, long-term X-ray pulsed-flux flares as well as short bursts, and large (>10×) torque changes. Monitoring with *RXTE* revealed that the source entered a phase of timing stability in 2004; at the same time, a series of four simultaneous observations with *CXO* and *HST* in 2006 showed that its X-ray flux and spectrum and near-IR flux, all variable prior to 2005, stabilized. Specifically, we find the 2006 X-ray spectrum to be consistent with a two-component blackbody plus power law, with average $kT = 0.52$ keV and power-law index $\Gamma = 2.8$ at a mean flux level in the 2−10 keV range of $\sim 6.5\times10^{-12}$ erg cm^{-2} s^{-1}. The near-IR flux, when detected by *HST* ($H \sim 22.7$ mag) and *VLT* ($K_S \sim 21.0$ mag), was considerably fainter than previously measured. Recently, in 2007 March, this newfound quiescence was interrupted by a sudden flux enhancement, X-ray spectral changes and a pulse morphology change, simultaneous with a large spin-up glitch and near-IR enhancement. Our *RXTE* observations revealed a sudden pulsed flux increase by a factor of ∼3 in the 2−10 keV band. In observations with *CXO* and *Swift*, we found that the total X-ray flux increased much more than the pulsed flux, reaching a peak value of >7 times the quiescent value (2−10 keV). With these recent data, we find a strong anti-correlation between X-ray flux and pulsed fraction. In addition, we find a correlation between X-ray spectral hardness and flux. Simultaneously with the radiative and timing changes, we observed a significant X-ray pulse morphology change such that the profile went from nearly sinusoidal to having multiple peaks. We compare these remarkable events with other AXP outbursts and discuss implications in the context of the magnetar model and other models of AXP emission.

Subject headings: pulsars: general — pulsars: individual (1E 1048.1−5937) — stars: neutron — stars: pulsars

1. INTRODUCTION

The small handful of unusual objects known as anomalous X-ray pulsars (AXPs) are characterized by their slow spin periods (5–12 s), large inferred magnetic fields (∼10^{14} G), and persistent X-ray luminosities in great excess of available spin-down power. These young, isolated pulsars have properties common to another class of objects, the soft gamma repeaters (SGRs). For recent reviews, see Woods & Thompson (2006) and Kaspi (2007). Potentially the most intriguing and most revealing property shared by AXPs and SGRs is their highly volatile nature: both are known to exhibit occasional and sudden dramatic flux and spin variability in the form of X-ray bursts, flares, and glitches.

The magnetar model (Duncan & Thompson 1992; Thompson & Duncan 1995; Thompson & Duncan 1996) was instrumental in explaining both the "anomalous" X-ray emission, as well the episodes of burst activity. It identified the sources as highly magnetized isolated neutron stars, with field strengths on the order of $10^{14} - 10^{15}$ G. The magnetar model uniquely, and correctly, predicted that SGR-like bursts would be observed from AXPs. A major proposed effect of this enormous magnetization is the "twisting" of the magnetosphere, with associated magnetospheric currents and heating of the crust at the twisted field-line footpoints (Thompson et al. 2002). This gives rise to the unusual X-ray spectrum, which has generally been empirically well characterized by a two-component model consisting of a power law plus blackbody. Bursts of high-energy emission occur presumably when the crust succumbs to magnetic stresses and deforms, leading to a rapid rearrangement of the external magnetic field. Recently, Beloborodov & Thompson (2007) proposed the existence of a plasma corona contained within the closed magnetosphere to explain the broad band spectrum of magnetars that extends from the infrared (IR) to hard X-rays beyond 100 keV (Kuiper et al. 2006).

1E 1048.1−5937 has had an unusual history, even by AXP standards[7]. Prior to 2002, monitoring of

[1] Department of Physics, Rutherford Physics Building, McGill University, 3600 University Street, Montreal, QC, H3A 2T8, Canada
[2] NASA Goddard Space Flight Center, Astrophysics Science Division, Code 662, Greenbelt, MD, 20771, USA
[3] NPP Fellow; Oak Ridge Associated Universities, Building SC−200, 1299 Bethel Valley Road, Oak Ridge, TN, 37830, USA
[4] Canada Research Chair; Lorne Trottier Chair; R. Howard Webster Fellow of CIFAR
[5] Dynetics, Inc., 1000 Explorer Boulevard, Huntsville, AL, 35806, USA
[6] NSSTC, 320 Sparkman Drive, Huntsville, AL, 35805, USA

[7] A summary of its properties can be found in the online SGR/AXP Catalog

the pulsed flux with the *Rossi X-ray Timing Explorer* (*RXTE*) showed that its spin down was so unstable that phase coherence could be maintained for periods of only months at a time (Kaspi et al. 2001), behaviour which echoed earlier reports of $\dot{P}$, flux and spectral variability (Oosterbroek et al. 1998). Two small bursts, the first ever found in an AXP, were discovered in 2001 from 1E 1048.1−5937 (Gavriil et al. 2002), clinching the suspected association between AXPs and SGRs. Since 2002, tri-weekly *RXTE* observations of 1E 1048.1−5937 allowed the changing pulsed flux and spin-down rate to be monitored on relatively short timescales. Gavriil & Kaspi (2004, hereafter GK04) reported order-of-magnitude torque variability on timescales of weeks to months that only marginally correlated with large luminosity variations. The unusually slow and long-lived pulsed flux "flares" (not to be confused with the SGR giant flares; see Woods & Thompson 2006) that began in late 2001 and lasted into 2004 are in some ways unlike activity seen in any other AXP or SGR thus far. The 2−10 keV spectrum and pulsed fraction are also variable on long timescales, the latter being anti-correlated with luminosity (Mereghetti et al. 2004; Tiengo et al. 2005). At near-infrared (near-IR) wavelengths, the flux varied dramatically during 2002−2003 (Wang & Chakrabarty 2002; Israel et al. 2002); unfortunately, the sparsity of near-IR observations prohibits measurements of the variability timescale, although a near-IR/X-ray anti-correlation has been suggested (Durant & van Kerkwijk 2005). Further activity in the form of another burst and small pulsed-flux increase was seen in 2004 (Gavriil et al. 2006).

Here, we report on a series of simultaneous *CXO* and *HST* observations obtained during the course of 2006, as well as on archival *CXO*, *XMM* and *VLT* observations, in § 2. We also present *RXTE* timing results from the past three years. In 2007 March, 1E 1048.1−5937 unexpectedly entered yet another new phase of activity, and we report on Target-of-Opportunity observations with *CXO* and *Swift* taken after the 2007 March event. In § 3.1 we discuss the 2004-2006 period of radiative and spin quiescence in the context of both magentar and accretion models, and in § 3.2, we describe and interpret the events following the 2007 March flare.

2. OBSERVATIONS, ANALYSIS AND RESULTS

As part of a long-term project, we regularly monitor AXPs using the *Rossi X-ray Timing Explorer* (*RXTE*). 1E 1048.1−5937 is by far the most frequently observed AXP due to its relatively poor rotational stability. The *RXTE* observations (see § 2.1) are crucial in measuring the spin evolution of the source and its pulsed flux. However, the high background and large unimaged field-of-view of *RXTE* make spectral measurements of 1E 1048.1−5937 difficult and total flux (and consequentially pulsed fraction) measurements impossible. To make these measurements, we obtained five *Chandra X-ray Observatory* observations (*CXO*; see § 2.2) approximately equispaced throughout 2006. In order to probe the origin of the near-IR emission of this source, we observed with the *Hubble Space Telescope* (*HST*; see § 2.3) simultaneously with *CXO*. The motivation for simultaneous *CXO* and *HST* observations was to search for correlated variability in the different bands, as that provides insight into the physical mechanisms generating the radiation. We also examined archival K_S-band observations with the *Very Large Telescope* (*VLT*; see § 2.4), which contribute to our monitoring of its near-IR brightness. Following the 2007 March glitch detected in our *RXTE* monitoring observations of 1E 1048.1−5937 (Dib et al. 2007b), we initiated three *CXO* and two *Swift Gamma-Ray Burst Explorer* (*Swift*; see § 2.2) Target-of-Opportunity (ToO) observations to follow the X-ray flux and spectrum of the source. In order to characterize the long-term evolution of 1E 1048.1−5937 we also incorporate and reanalyze archival *XMM-Newton* and *CXO* observations (see Gavriil et al. 2006, for details on how these data were processed). Separate post-outburst optical and near-IR observations of 1E 1048.1−5937 are reported in detail elsewhere (Wang et al. 2007).

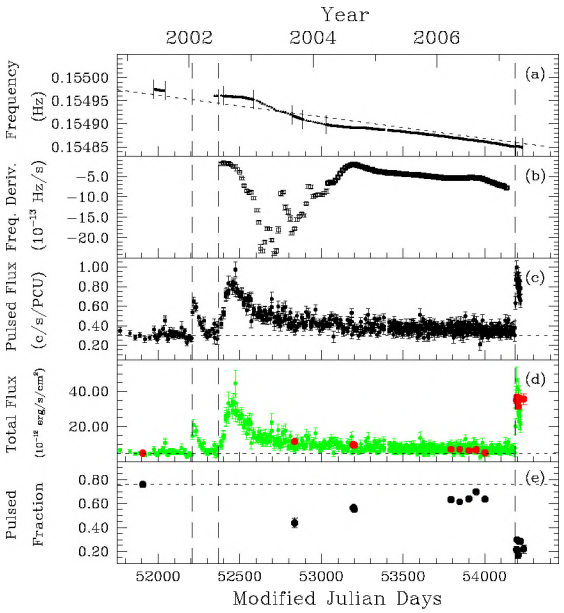

FIG. 1.— The long-term evolution of 1E 1048.1−5937's pulsed properties. The three vertical dashed lines indicate the approximate beginnings of the flux flares on (from left to right) 2001 October 26, 2002 April 6, and 2007 March 21, respectively. Horizontal dotted lines represent the value of the plotted parameter prior to all observed flares. (*a*) Spin frequency as observed by *RXTE*. Small points show the measured frequencies, while intervals over which phase coherence has been maintained are shown as thick lines (GK04; Dib et al., in preparation). (*b*) Frequency derivative as a function of time. While the frequency was varying in 2002-2004 and a phase-coherent timing solution could not be found, $\dot{\nu}$ was determined in short intervals by calculating the slope of three consecutive ν measurements (after GK04). Since 2004, phase coherence has been maintained and $\dot{\nu}$ reflects the standard technique (Dib et al., in preparation). (*c*) 2−10 keV rms pulsed flux as observed by *RXTE*. (*d*) Simulated total 2−10 keV unabsorbed flux, shown as green points. Total flux is estimated from the *RXTE* pulsed flux and the power-law correlation between pulsed fraction and measured total flux, shown as red points, as described in § 3.2.2. The simulated fluxes (*green*) have been scaled to match the actual measured total fluxes (*red*). (*e*) 2−10 keV rms pulsed fraction calculated using the method described in Woods et al. (2004).

2.1. *RXTE*

We have observed 1E 1048.1−5937 regularly since 1997 with *RXTE* (Kaspi et al. 2001; GK04). Our data were obtained using the Proportional Counter Array (PCA) on board *RXTE* which consists of five identical

http://www.physics.mcgill.ca/∼pulsar/magnetar/main.html.

and independent Xenon/Methane Proportional Counter Units (PCUs). We use our *RXTE* observations of 1E 1048.1−5937 to look for the presence of bursts (see Gavriil et al. 2004 for details), to look for pulse profile changes, to monitor its pulsed flux, and to monitor its frequency evolution using phase-coherent timing when possible.

For the timing analysis, we created barycentered lightcurves in the 2−5.5 keV band with 31.25 ms time resolution. As past monitoring has shown that it can be difficult to maintain pulse phase coherence over timescales longer than a few weeks, observations of 1E 1048.1−5937 since 2002 are done three times per week, with the three observations carefully spaced so as to allow a phase-coherent analysis and a precise frequency measurement. Thus, for each observation, we fold at the pulse period determined via periodogram, cross-correlate the folded profiles with a high signal-to-noise template, and fit the resulting phases with a linear function whose slope provides the average frequency. Frequencies determined in this way are shown in Figure 1. As can be seen in this figure, the 2004-2006 frequencies were actually much more stable than in the past; we therefore attempted a fully phase-coherent analysis as well. This will be described elsewhere (Dib et al., in preparation). Frequency derivatives, which are also displayed in Figure 1 and are from GK04 and Dib et al., (in preparation), are clearly much more stable in the 2004-2006 interval than previously.

This period of rotational stability was accompanied by X-ray pulsed flux stability and relative quiescence: the pulsed flux time series of 1E 1048.1−5937 in the 2−10 keV band is presented in Figure 1. The pulsed flux was calculated using a method similar to that described in Woods et al. (2004) and is based on the rms of the folded profile, but without variance subtraction.

The long period of rotational stability ended in 2007 March, when a large glitch was observed (Dib et al. 2007b). The glitch also signaled the end of the period of pulsed flux quiescence. The pulsed flux suddenly increased by a factor of ∼3 in the energy range 2−10 keV. The upper limit on the rise time of the pulsed flux for this event is approximately one week. The peak pulsed flux reached by the source was ∼10% larger than the peak flux reached during the largest of the two previously observed flares, and the rise time was at least 4 times smaller. On 2007 May 17, the date of the last X-ray imaging observation included in this paper, the pulsed flux had decreased by ∼10%. It is as yet difficult to compare the decay timescale of the pulsed flux of this new event to that of the previous flares however it will be possible in the near future.

2.2. *CXO and Swift*

X-ray imaging observations were carried out with the *CXO* and *Swift* telescopes. The date, total exposure time and resulting count rate for each region-filtered background-subtracted observation are listed in Table 1 and a detailed description of our spectral fitting is given in § 2.2.1.

1E 1048.1−5937 was observed five times[8] in 2006 with

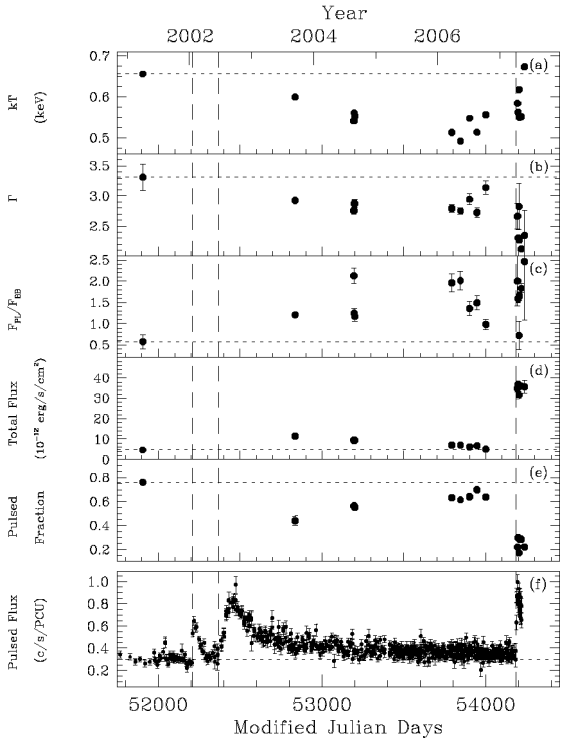

FIG. 2.— The evolution of 1E 1048.1−5937's X-ray spectral properties. For consistency, all the spectra from *CXO*, *Swift*, and *XMM* were fit jointly with a two-component absorbed blackbody plus power-law model, that produced a best-fit $N_H = (0.97 \pm 0.01) \times 10^{22}$ cm^{-2} (see § 2.2.1). The uncertainties shown reflect statistical errors only. Vertical dashed lines indicate the beginnings of the flux flares (see Fig. 1 caption), while horizontal dotted lines indicate quiescent values. (*a*) Blackbody temperature kT. (*b*) Photon index Γ. (*c*) Ratio of the 2−10 keV flux contribution from the blackbody and power law components. (*d*) Total unabsorbed flux in 2−10 keV. (*e*) 2−10 keV rms pulsed fraction calculated using the method described in Woods et al. (2004). (*f*) For reference, we show the 2−10 keV rms pulsed flux as observed by *RXTE*.

CXO in quasi-equispaced intervals, and three times in 2007 April. The observations were made with the Advanced CCD Imaging Spectrometer (ACIS) camera using the S3 chip in continuous clocking (CC) mode. This mode generates a 1×1024 pixel image, which is read out every 2.8 ms; pile-up in this mode is not an issue. The subsequent analysis was based on the "Level 2" events files for which the event times are photon arrival times (as opposed to readout times for the "Level 1" events). Following the standard threads we then corrected the "Level 2" events for certain caveats related to ACIS CC-mode data[9]. We extracted a rectangular region centered on the source with a width typically of ∼30 pixels. We estimated the background using rectangular regions on either side of the source which extended from ∼10 pixels beyond the edge of the source region to ∼10 pixels from the edge of the image. Following the standard threads, the source and background spectra were then extracted using `CIAO`[10] v3.4. We grouped the source spectrum such that there were no fewer than 20 counts per bin after background subtraction. The response matrix function (rmf) and area response function (arf) for each observation were also generated using `CIAO` and `CALDB`. We used Timed Exposure (TE) mode response matrices because

[8] Although four simultaneous observations were originally planned, *HST* experienced technical difficulties during one, resulting in a fifth *CXO* observation.

[9] `http://cxc.harvard.edu/ciao3.4/why/ccmode.html`

[10] `http://cxc.harvard.edu/ciao`

of the absence of available spectral calibration for CC mode.

1E 1048.1−5937 was observed three times[11] in 2007 with *Swift* using the X-ray Telescope (XRT). XRT has two observing modes: photon counting (PC) and windowed-timing (WT). PC mode provides a ∼600×600 pixel^2 image with low (∼2.5 s) time resolution, whereas WT mode provides a one-dimensional ∼200-pixel wide image with high (∼0.74 ms) time resolution. XRT automatically switches from WT to PC-mode when the count rate exceeds ∼2 counts s^{-1}. In our analysis we ignored the WT mode data as they were too short to be of use. We used the PC-mode event files from the standard pipeline; these were cleaned and barycentered. Using `FTOOL xrtcentroid`, we determined the centroid of the image, and input the cleaned, barycentered events into the command line interface `xselect`[12]. We selected a circular source region with a 25 pixel radius centered on the centroid of the image. Since the source was slightly piled up, we excluded a 4 pixel radius circular region centered on the centroid of the image. We used 4 pixels because that is the recommended exclusion radius for a source with 1E 1048.1−5937's spectrum (L. Angelini, private communication). For the background, we selected events from an annulus with an inner radius of 50 pixels and outer radius of 130 pixels. We further filtered our events by selecting only those that had grades 0 to 12. With `xselect` we then created source and background PHA files. The `FTOOL xrtmkarf` was used to create the arfs, and we input the source PHA file with the excluded center so that it would be corrected for pile-up. We used the file provided by `CALDB` appropriate for PC mode data events of grades 0 to 12 to make the rmf.

2.2.1. *Global Spectral Fit*

We extracted spectra of 1E 1048.1−5937 from all archival, monitoring, and ToO observations collected from *CXO*, *XMM* and *Swift*. A description of the recent data analysis is in § 2.2, and the archival analysis was described in Gavriil et al. (2006). Using the fitting package `XSPEC`[13] v12.3.1 we modeled the X-ray spectra with a photoelectrically absorbed blackbody plus power law. We used the `phabs` photoelectric absorption `XSPEC` model, which assumes the solar abundance table of Anders & Grevesse (1989) and uses the `bcmc` photoionization cross-section table from Balucinska-Church & McCammon (1992) with the new He cross-section from Balucinska-Church & McCammon (1998). We fit this model to all the observations simultaneously, allowing the column density N_H to vary but with the sole constraint that it be the same for all observations. We restricted our fit to the 0.7–5 keV band. The total global fit had $\chi^2_\nu = 1.07$ for $\nu = 4200$ degrees of freedom (dof). Individually, the observations were equally well modeled (except for a relatively high χ^2 value in one observation, see § 2.2.2). Our best-fit column density obtained from the global fit is $N_H = (0.97 \pm 0.01) \times 10^{22}$ cm^{-2}, in agreement with Durant & van Kerkwijk (2006b). The results of our spectral fitting are listed in Table 1 and plotted in Figure 2.

2.2.2. *Possible Spectral Feature*

All observations had spectra that were well modeled by a photoelectrically absorbed blackbody plus power law. However, the *CXO* observation on 2007 April 6 (observation ID 7647), the first after the 2007 March event, had a relatively high $\chi^2_\nu = 1.33$ ($\nu = 353$ dof). There is possible evidence for an absorption line at ∼2.7 keV (see Fig. 3). Adding a Gaussian line improved the fit ($\chi^2_\nu = 1.20$ for $\nu = 351$ dof) with $\Delta\chi^2 = 48.3$. With the line width fixed at 0.1 keV, we measure a line energy of 2.73 ± 0.03 keV. Allowing the line width σ to be a free parameter, we obtain $\sigma = 0.16 \pm 0.03$ keV, a line energy of 2.74 ± 0.03 keV and $\chi^2_\nu = 1.19$ for 351 dof. We find no evidence of a phase dependence for this possible line. A detailed phase-resolved spectroscopic analysis will be presented in a forthcoming paper.

To test the significance of adding such a line, we performed the following simulation. We generated 10000 simulated spectra by adding Poisson noise to a blackbody plus power-law model spectrum having the same parameters as our best-fit model. We then determined the maximum change in χ^2 after adding a Gaussian line. To avoid local minima and ensure that we found the true minimum χ^2 for each simulation iteration, instead of fitting for the peak energy, we stepped through different line energies between 0.6 and 7.0 keV with a step size of 0.025 keV. The width of each line was held fixed at 0.1 keV and its normalization was allowed to vary. In all the simulation iterations, none had a change in χ^2 greater than 48.3. The probability that this feature is due to random chance is <0.13%, accounting for the number of trials. We note however that with the addition of the line, the overall fit is still unacceptable; we speculate that other features may be present as well, though at marginal significance. For example, there is a small but intriguing feature at ∼1.3 keV, which is approximately half the energy of the line discussed above. The evidence for a line must be considered tentative because CC mode, which uses the TE mode response matrices, is not spectrally calibrated, and there exist calibration lines between 1.7 and 3 keV in the TE response. However, this is true for the other *CXO* observations, including those in which we find no such features.

2.2.3. *Pulse Morphology and Pulsed Fraction Study*

Using our *CXO* and *Swift* observations we were also able to study the source's pulse morphology, flux and pulsed fraction.

For the *CXO* observations, we barycentered our corrected Level 2 event lists and then extracted background-subtracted light curves in the different bands using the same source and background regions as for the spectral analysis. We folded these lightcurves at the optimal frequency as determined by a periodogram. The frequencies we obtained all agreed with the ephemerides determined with our contemporaneous *RXTE* data. Figure 4 (*left*) displays the *CXO* pulse profiles in the 1−3 and 3−10 keV bands. Notice that after the flare (last 3 panels in Figure 4 *left*), the pulse profile changed from single to at least triple peaked. To study the pulse morphology evolution quantitatively we decomposed the pulse profiles

[11] Two additional *Swift* observations taken contemporaneously were omitted from our analysis because their short exposures yielded prohibitively large uncertainties.

[12] `http://heasarc.gsfc.nasa.gov/docs/software/lheasoft/ftools/xselect/xselect.html`

[13] `http://xspec.gsfc.nasa.gov`

TABLE 1
CXO, *XMM* AND *Swift* OBSERVING PARAMETERS AND RESULTS

Date	MJD	Obs. ID	Exposure (s)	Count rate (counts s^{-1})	Γ^a	kT^a (keV)	Unabs. Flux^{a,b} (10^{-12} erg cm^{-2} s^{-1})	$F_{PL}/F_{BB}{}^{a,c}$	Pulsed Fraction^d
Archival *XMM* Observations									
2000 Dec 28	51906	0112780401	4447	1.461(18)	3.31(22)	0.656(17)	4.8(4)	0.6(2)	0.76(2)
2003 Jul 16	52836	0147860101	41145	3.429(9)	2.93(4)	0.599(6)	11.5(1)	1.21(5)	0.44(4)
2004 Jul 9	53195	0164570301	32679	0.985(6)	2.75(5)	0.542(15)	9.6(1)	2.1(2)	0.561(7)
Archival *CXO* Observations									
2004 Jul 10	53196	4653	28860	1.363(7)	2.87(7)	0.56(1)	9.3(1)	1.2(1)	0.56(1)
2004 Jul 15	53201	4654	28085	1.317(7)	2.87(7)	0.55(1)	9.4(2)	1.2(1)	0.55(1)
Monitoring *CXO* Observations									
2006 Feb 26	53792	6733	22085	1.072(8)	2.79(6)	0.51(1)	7.1(1)	2.0(2)	0.63(1)
2006 Apr 20	53845	6734	20553	1.157(9)	2.75(5)	0.50(1)	7.1(2)	2.0(2)	0.61(1)
2006 Jun 14	53900	6735	22085	0.985(9)	2.95(9)	0.55(1)	6.3(1)	1.4(2)	0.64(1)
2006 Jul 30	53946	7347	22176	0.821(8)	2.72(8)	0.51(1)	6.8(2)	1.2(2)	0.70(1)
2006 Sep 23	54001	6736	22022	1.006(7)	3.14(11)	0.56(1)	5.1(1)	1.0(2)	0.64(1)
ToO *CXO* Observations									
2007 Apr 6	54196	7647	20079	4.241(15)	2.30(4)	0.56(1)	36.9(5)	1.6(1)	0.299(5)
2007 Apr 16	54206	7648	18387	3.959(15)	2.27(4)	0.55(1)	36.0(5)	1.7(1)	0.286(6)
2007 Apr 28	54218	7649	19082	4.332(15)	2.12(4)	0.55(1)	36.0(5)	1.8(1)	0.287(5)
ToO *Swift* Observations									
2007 Apr 3	54193	30912001	4905	0.58(1)	2.7(2)	0.58(6)	35(2)	2.0(6)	0.22(3)
2007 Apr 13	54203	30912003	4829	0.55(1)	2.8(4)	0.62(4)	32(2)	0.7(3)	0.17(3)
2007 May 17	54237	30912009	3626	0.51(1)	2.3(4)	0.7(1)	35(3)	2(1)	0.22(3)

NOTE. — All quoted errors represent 1σ uncertainties. The archival *XMM* and *CXO* observations have been previously reported by Mereghetti et al. (2004), Tiengo et al. (2005), and Gavriil et al. (2006).
[a] These results are from a simultaneous spectral fit to all the data using as a model a photoelectrically absorbed blackbody with temperature kT and a power law with photon index Γ. In the simultaneous fit the column density, N_H, was constrained to be the same for all observations. The resultant N_H from the global fit was $N_H = (0.97 \pm 0.01) \times 10^{22}$ cm^{-2}; see the text for details.[b] Total unabsorbed flux in the 2−10 keV band.[c] Ratio of the 2−10 keV flux in the power-law component, F_{PL}, to the 2−10 keV flux in the blackbody component, F_{BB}.[d] 2−10 keV pulsed fraction, using the definition of pulsed fraction described in Woods et al. (2004).

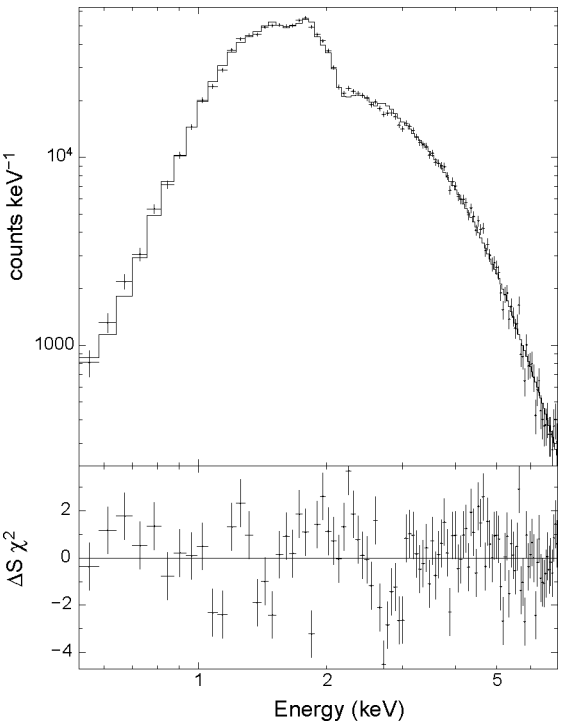

FIG. 3.— 1E 1048.1−5937's X-ray spectrum on 2007 April 6, as observed by *CXO*. *Top*: The best-fit photoelectrically absorbed blackbody plus power law is plotted as a solid line; see text for details on the analysis. The quality of the fit was low, with $\chi^2_\nu = 1.33$ for $\nu = 353$ dof. *Bottom*: Residuals after subtracting the best-fit model. Notice a possible spectral feature at ∼2.7 keV.

into their Fourier components. In Figure 4 (*right*) we plot the Fourier components in terms of their ratio to the fundamental (the $n = 0$ and fundamental are excluded from the plot). Notice that before the flare the profile consisted only of the fundamental and an $n = 2$ Fourier component. After the flare, the profile exhibited significant Fourier components of order $n = 2, 3, 5$. Interestingly, despite the drastic changes in the other Fourier components, the $n = 4$ component remains consistent with zero throughout the flare.

Similarly, for the *Swift* observations we used the barycentered, cleaned, and pointed PC-mode data events. The XRT WT data consisted of too few pulses to be useful. *Swift* PC-mode data have only 2.5-s resolution, providing fewer than 3 pulse phase bins for this 6.45-s pulsar. We attempted to improve on the coarse sampling by utilizing advanced "bin splitting" techniques (G. Israel, private communication), however we find only marginal evidence for a pulse profile change from these data (but see Campana & Israel 2007).

Using our folded pulse profiles we measured root-mean-square (rms) pulsed fractions[14] using the method described in Woods et al. (2004). Our 2−10 keV rms pulsed fractions are listed in Table 1 and plotted in Figures 1 and 2. The *XMM* pulsed fractions, taken from Gavriil et al. (2006), were extracted in the same fashion. Because of the low time resolution of the *Swift* data, the rms pulsed fraction would be artificially reduced if the pulse contained as much harmonic content as the *CXO* data during the flare. Thus, for each *Swift* observation we simulated, given its observed pulsed fraction and mean

[14] For a simple signal of the form $c(\phi) = A\sin(2\pi\phi) + B$, the rms pulsed fraction is given by $PF_{\rm rms} = \frac{1}{\sqrt{2}}\frac{A}{B}$, and the peak-to-peak pulsed fraction is given by $PF_{\rm pp} = \frac{A}{B}$. We opted to use the rms with Fourier filtering (Archibald et al., in preparation) because it is a more robust estimator of the pulsed fraction than peak-to-peak.

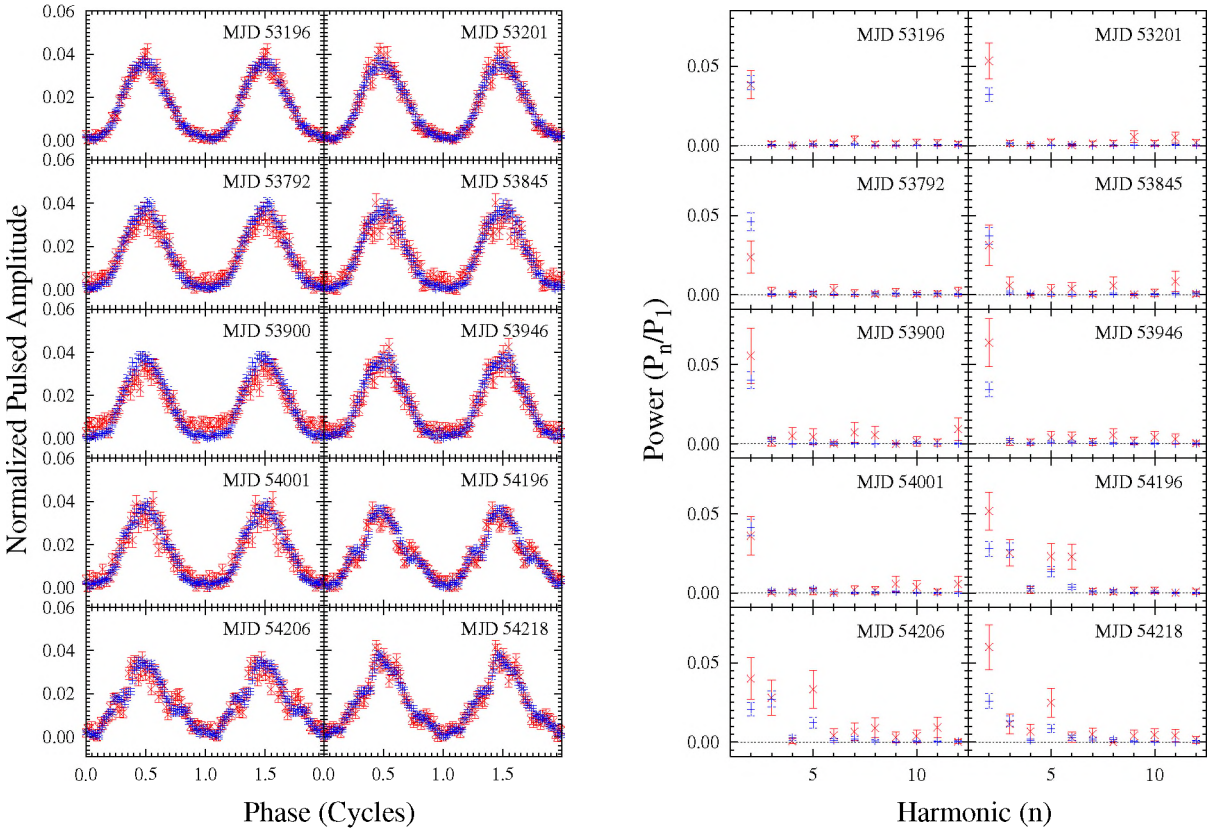

FIG. 4.— *Left*: 1−3 keV (*blue*) and 3−10 keV (*red*) normalized pulsed profiles as observed by *CXO*. The profiles are phase aligned, have had their minimum bins subtracted, and are normalized such that the area underneath them is unity. Note that the 2007 event occured around MJD 54183. *Right*: 1−3 keV (*blue*) and 3−10 keV (*red*) Fourier decomposition of the pulse profiles. The powers P_n are plotted in terms of their ratio to the fundamental P_1. The $n = 0$ and the $n = 1$ (fundamental) components are excluded. Notice how the pulse profile has additional structure after the glitch/flux enhancement.

count rate, what its true pulsed fraction would be assuming a pulse profile with as much harmonic content as the nearest *CXO* observation. On average we found a reduction of no more than ∼73%. Note in Figure 2 the observed tight correlation between total flux and pulsed fraction (see also Tiengo et al. 2005) which we discuss in detail in § 3.2.2.

2.3. *HST*

We observed 1E 1048.1−5937 using *HST* simultaneously with *CXO* on four occasions in 2006: February 26, April 20, July 30, and September 23 (Program ID 10761). Observations were made with the Near Infrared Camera and Multi-Object Spectrometer (NICMOS) instrument, a 256 × 256 square pixel HgCdTe detector. Combined with camera 3, it provided a focus ratio of $f/17$, a field of view of $51'\times51'$, and a plate scale of $0\farcs2$ pixel^{-1}. The detector was read out in MULTIACCUM mode, and a spiral dither pattern with $5''$ spacings was applied. We observed using the filter F110W (similar to the ground based J-band filter) on two occasions and F160W (similar to H-band) on four occasions. The average FWHM of the point spread function (PSF) was $\sim 0\farcs4$ for all NICMOS observations. Observing parameters are summarized in Table 2.

The data underwent "On-The-Fly-Reprocessing" involving standard pipeline routines before being retrieved from the *HST* Archive. The calibration routine `calnica` performed basic data reduction steps, and `calnicb` produced a single final image for each observation, com-

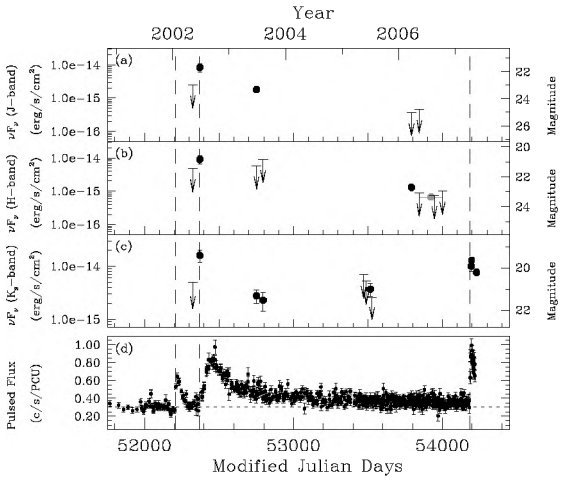

FIG. 5.— The evolution of 1E 1048.1−5937's near-IR brightness. *VLT* and *HST* results from this work fall after 2004, while data prior to that are from previous literature (Wang & Chakrabarty 2002; Israel et al. 2002; Durant & van Kerkwijk 2005). We also show the corresponding magnitude on the right axis; however the translation is not exact due to *HST*'s unique filters. Vertical dashed lines indicate the beginnings of the flux flares (see Fig. 1 caption), while horizontal dotted lines indicate quiescent values. (*a*) "J-band" flux νF_ν. (*b*) "H-band" flux νF_ν. The detection made from combining three *HST* observations (see § 2.3) is shown in grey. (*c*) "K_S-band" flux νF_ν. Results from 2007 are described in detail elsewhere (Wang et al. 2007). (*d*) For reference, we show the 2−10 keV rms pulsed flux as observed by *RXTE*.

bining the dithered mosaic input images. DAOPHOT (Stetson 1987) for IRAF v2.12.2 was used to perform PSF photometry. Absolute calibration of our measurements was done using the NICMOS Photometric Keywords[15] for which the uncertainties are believed to be less than 5%; we found the aperture correction to correspond with the calibration keywords by simulating PSFs with the Tiny Tim[16] software package.

In order to determine limiting instrumental magnitudes in each of the observations, we performed PSF photometry on a set of a hundred trial images to which a single artificial star was added. This artificial star was placed in a 0.″3 box in a blank region near the nominal position of the IR counterpart. By varying the brightness of the star, we define the 3σ detection limit at the instrumental magnitude for which the PSF photometry recovers the artificial star with an uncertainy of 0.3 mag (see Hulleman et al. 2000).

At the position of 1E 1048.1−5937, as measured by Wang & Chakrabarty (2002) in K_S-band with the *Magellan* telescope, we find one point source in the F160W image from 2006 February 26 only. To confirm the positional coincidence of this source with the *Magellan* object, we astrometrically tied $N = 31$ nearby field stars in our *HST* image to those from the *Magellan* image. A $\sim$ 0.″05 offset was found for the 1E 1048.1−5937 candidate. The *Magellan* source's relative positional uncertainty, given its 0.″4 FWHM radius, is roughly FWHM/$\sqrt{N}$ $\sim$ 0.″07. Therefore, we consider this *HST* object the counterpart of 1E 1048.1−5937.

Thus, we measure our lone detection of 1E 1048.1−5937 to have $m_{F160W} = 22.70 \pm 0.14$ mag; uncertainties indicate the nominal errors determined by DAOPHOT and incorporate PSF fitting uncertainties. Limiting magnitudes for the three latter *HST* F160W observations in which no counterpart was seen are presented in Table 2. To deepen the sensitivity, geometric transforms were computed to register and combine the three non-detection datasets. In the combined data, we tentatively detect an extremely faint counterpart of brightness $m_{F160W} = 23.42 \pm 0.20$ mag, where the 3σ upper limit is $>$ 23.5 mag. We find no F110W counterpart down to a 3σ upper limit of $m_{F110W} > 25.0$ mag and > 24.8 mag, on February 26 and April 20, respectively. Results are plotted in Figure 5.

To examine how this compares with past results, we also calibrated our measurements using the H magnitudes from Durant & van Kerkwijk (2005). A relative offset is found between *HST*'s F160W filter and ground based H-band, as a function of $J - H$ color. We know the color of 1E 1048.1−5937 only during a brightened state ($J - H \approx 0.9$ in April 2002; Wang & Chakrabarty 2002), and suspect that it is not constant; therefore, this is not a perfect comparison, but provides a rough estimate. Based on the magnitudes of seven nearby field objects, we measure $H \approx 22.73$ mag on February 26, which is very near what we find for m_{F160W}.

2.4. *VLT*

We have analyzed archival observations of 1E 1048.1−5937 which were obtained with NAOS-CONICA (NACO), the near-IR adaptive optics (AO) instrument at *VLT* of the European Southern Observatory. The source was observed for 900 s in K_s-band using the S27 camera ($28'' \times 28''$ field-of-view and 27 mas pix^{-1} pixel scale) on four occasions (April 11, April 29, May 27 and June 6) in 2005. Star A (Wang & Chakrabarty 2002), located 9.″5 from the AXP, was used as the wavefront-sensing (WFS) star. Due to the relative faintness of the WFS star ($r' = 16.5$ mag), the AO correction was only partial.

The observations, either dithered sets of 5 2×90 s integrations (on the first night) or of 10 1×90 s integrations, were corrected for dark current, flat-fielded (using averages derived from the science frames) and corrected for variations in the sky (using median averages of the flat-fielded science frames). Finally, the reduced science images were aligned using integer pixel offsets and median-combined to create an average image for each night.

Using DAOPHOT, we tried PSF photometry on each of the four averaged images, using different models for the PSF. Because the AO correction is only partial, we found that the PSF is reasonably well modeled by a Moffat function of exponent 2.5 in combination with a look-up table. The width of the PSF that was determined for each observation was 0.″34 (April 11), 0.″43 (April 29), 0.″24 (May 27) and 0.″20 (June 6). Only in the observation of May 27 did we detect the near-IR counterpart to 1E 1048.1−5937.

We calibrated the instrumental magnitudes and magnitude limits using stars X2 to X8 and A and B against the calibrated K_s magnitudes of Wang & Chakrabarty (2002). The rms uncertainty in the calibration is about 0.2 mag. The near-IR counterpart to 1E 1048.1−5937 was detected at $K_s = 21.0 \pm 0.3$ on 2005 May 27; the 3σ upper limits for April 11, April 29, May 27 and June 6 are $K_s > 20.3$, $K_s > 20.6$, $K_s > 21.2$ and $K_s > 21.4$, respectively. Limiting magnitudes were determined with the same method described in § 2.3. Results are shown in Figure 5.

Note that post-2007 event optical and near-IR observations of 1E 1048.1−5937 were obtained with *VLT* and *Magellan* (Wang et al. 2007; Israel et al. 2007). Preliminary results of the K_S-band observations are shown in Figure 5, and details on some of the observations can be found in Wang et al. (2007).

3. DISCUSSION

Explaining the origin of the different types of AXP variability across the electromagnetic spectrum is a major challenge for the magnetar model. Many fundamental questions remain open. In the case of 1E 1048.1−5937, how are timing instabilities related to radiative variability? AXP spin-up glitches sometimes are accompanied by major radiative events, as in the 2002 outburst of AXP 1E 2259+586 (Kaspi et al. 2003), and sometimes not, as in the large glitch of 1E 1841−045 (Dib et al. 2007a). Moreover, are the *gradual* large-scale changes seen in the 2001-2002 flares of 1E 1048.1−5937 of a similar origin to AXP outbursts like that of 1E 2259+586 or XTE J1810−197 (Ibrahim et al. 2004), and how can they be accounted for by magnetar models? Also, what is the nature of the optical/IR emission observed in five out of eight confirmed AXPs? Suggested origins include coherent or curvature emission in the plasma magne-

[15] http://www.stsci.edu/hst/nicmos/performance/photometry
[16] http://www.stsci.edu/software/tinytim/tinytim.html

TABLE 2
HST AND *VLT* OBSERVING PARAMETERS AND RESULTS

Date	MJD	Exposure (s)	Filter[a]	Limiting Magnitude	Detection	νF_ν[b] (10^{-15} ergs s^{-1} cm^{-2})
VLT Observations						
2005 Apr 11	52324	900	K_S	>20.3	···	<7.0
2005 Apr 29	53471	900	K_S	>20.6	···	<5.3
2005 May 27	53489	900	K_S	>21.2	21.0(3)	<3.1; 3.7±1.0
2005 Jun 6	53527	900	K_S	>21.4	···	<2.6
HST Observations						
2006 Feb 26	53792	2637	F110W	>25.0	···	<0.37
2006 Feb 26	53792	1196	F160W	>23.7	22.70(14)	<0.49; 1.3±0.2
2006 Apr 20	53845	2637	F110W	>24.8	···	<0.45
2006 Apr 20	53845	1196	F160W	>23.1	···	<0.89
2006 Jul 30	53946	1037	F160W	>23.3	···	<0.74
2006 Sep 23	54001	1037	F160W	>22.9	···	<1.0

NOTE. — Magnitude uncertainties reflect errors determined by DAOPHOT; upper limits are 3σ limits, as defined in the text. Measured quantities are "observed", ie. have not been corrected for reddening/extinction effects.
[a] Although the filter system of *HST* does not precisely match standard ground-based near-IR filters, note that F110W $\approx$ J-band and F160W $\approx$ H-band.[b] To convert standard IR magnitudes to flux, we take as the $K_S = 0$ mag zero point $\nu F_\nu = 9.28 \times 10^{-7}$ ergs s^{-1} cm^{-2}, derived from Cox (2000). *HST* fluxes are determined from NICMOS Photometric Keywords.

tosphere (Eichler et al. 2002; Beloborodov & Thompson 2007), but so far this has not be confirmed. Are the low- and high-energy emission mechanisms intimately connected (Heyl & Hernquist 2005)? Correlated post-burst flux decay in the X-ray and near-IR regimes has been seen in at least one other AXP (Tam et al. 2004).

Given the many observational properties that have been characterized for 1E 1048.1−5937 in this work and for other AXPs in similar studies, which property will emerge as being the most constraining of physics is hard to know. The most promising behaviors are those which show clear correlations with others, or those that are common to many or all AXPs and SGRs. In this section, we discuss the behavior of 1E 1048.1−5937, and focus on the phenomena that are potentially the most useful for testing the magnetar or other competing models. We first consider the quiescent phase we have observed in 2004-2006, and its implications for AXP models, then subsequently discuss the source's return to activity in 2007 March.

3.1. *The 2004-2006 Quiescent Phase*

3.1.1. *X-ray Flux and Spectrum*

The X-ray flaring observed pre-2004 contrasts strongly with the stable pulsed fluxes we observed in 2004-2006 (Fig. 1*c*). Clearly the source's stable state is also its faintest. The X-ray spectrum during this quiescent phase is also fairly constant, with kT evolving post-flare, on a time scale of several years. Interestingly, kT does not return to its pre-flare value as measured in 2000 December (see Fig. 2*a*). Similarly, the photon index (Fig. 2*b*) decreased in 2004-2006, away from its softer pre-flare value. Meanwhile the pulsed fraction (Figs. 1*e* and 2*e*) was slowly rising in 2004-2006, as the source grew fainter, as if, unlike kT and Γ, it was slowly recovering to the pre-flare value. Thus, overall, the quiescent period is characterized by slow evolution, on timescales of years, in which the source flux and pulsed fraction slowly relaxed back to their pre-flare values, while the source spectrum varied significantly (Fig. 2*c*) and did not relax back to its pre-flare state. This is suggestive of a fixed energy loss rate in quiescence, though perhaps with a different magnetospheric current configuration, which impacts the surface emission via return currents (Thompson et al. 2002). We note, on the other hand, that the 2006 and pre-2001 pulse profile were very similar if not identical (Kaspi et al. 2001), and that the Thompson et al. (2002) simple prediction for the decay time of the sort of magnetospheric twist required for 1E 1048.1−5937 is an order of magnitude too large for standard parameters. The evolution could also be purely due to the thermal component (Özel & Guver 2007).

3.1.2. *Timing Stability*

Simultaneous with the slow evolution of the X-ray flux, pulsed fraction, and spectrum, the pulsar's rotational behavior clearly stabilized, with the source spinning down relatively smoothly at a value close to the long-term average in 2004-2006 (Fig. 1*a*). Whereas previously this AXP distinguished itself from others by defying attempts at phase-coherent timing and exhibiting large torque variations (Fig. 1*b*), in 2004-2006, 1E 1048.1−5937 resembled, from a timing point of view, other AXPs which are relatively stable rotators, at least when not glitching (e.g. Kaspi et al. 1999; Dib et al. 2007a). This behavior demonstrates a clear relationship between timing and radiative properties, and that the "noise" seen in the frequency derivative during 2001-2004 is likely physically different from the "timing noise" observed ubiquitously in radio pulsars and in otherwise radiatively stable AXPs.

In the context of the magnetar model, magnetospheric activity can account for both torque and X-ray flux variability, although the former is most sensitive to currents anchored closest to the magnetic poles, so that only a broad correlation between flux and torque is expected (Thompson et al. 2002) and indeed is seen when considering many AXPs and SGRs (Marsden & White 2001). That the torque and luminosity in 1E 1048.1−5937 do not vary simultaneously or in a clearly correlated way is thus not necessarily problematic if the magnetospheric current configuration is changing, although it does demonstrate that the magnetar model in this particular regard is not strongly predictive.

Although the magnetar model is favored, it has also been suggested that accretion from a fossil debris disk could explain AXP spin characteristics (Chatterjee et al. 2000; Alpar 2001) as well as all aspects of the broad band emission (Ertan & Çalışkan 2006). While it is now evident that accretion alone cannot be responsible for all observed properties, most notably the energetic X-ray bursts, a "hybrid" model has been invoked that puts a thin debris disk around a highly magnetized pulsar (Ekşı & Alpar 2003). In this hybrid case, both the persistent luminosity and pulsar spin down are related to the mass transfer rate, $\dot{M}$. According to GK04, who compare 1E 1048.1−5937's torque changes with changes in *RXTE* pulsed flux, the scale of their variability does not obey an expected relationship for an accreting pulsar undergoing spin-down, thus presenting a challenge to models of fossil disk accretion. It could be argued, however, that since only the pulsed flux P_X was being monitored, the total X-ray luminosity L_X is still an unknown quantity. We address this by using the quantitative correlation we establish between pulsed fraction $\mathcal{P}_\mathcal{F}$ and total unabsorbed flux F_X (discussed in § 3.2.2 and shown in Fig. 6) to simulate a well sampled set of phase-averaged flux data as a function of *RXTE* pulsed flux P_X, given that $\mathcal{P}_\mathcal{F}$ is simply P_X/F_X. The resulting "new" total flux, F_X, is shown in Figure 1*d*, along with $\dot{\nu}$ in Figure 1*b* for comparison. At its most variable in 2002-2004, the absolute value of $\dot{\nu}$ changed by a factor of >10 in less than a year, while the maximal change in total unabsorbed flux is a factor of ∼6 from peak to quiescence. Note that these variations are not simultaneous. For a pulsar experiencing a spin-down torque due to mass accretion while in a quasi-equilibrium "tracking" phase (i.e. the AXP phase), a strong correlation described by $L_X \propto |\dot{\nu}|^{7/3}$ can be derived from Chatterjee et al. (2000, equation 3), where the magnitudes of torque and $\dot{\nu}$ are proportional, the radius of the magnetosphere is defined by the Alfèn radius which is also a function of $\dot{M}$, and $L_X \propto \dot{M}$. Thus, a factor of >10 change in $\dot{\nu}$ should be reflected by a factor of >200 simultaneous change in L_X, and thus F_X, if this model is correct. Clearly this is not observed, rendering this particular accretion scenario unlikely. This point is further emphasized by the significant time offset between the changes in torque and flux. Overall, the fact that 1E 1048.1−5937's long history of highly irregular spin-down is mirrored by trends in its X-ray emission only in a broad, rather than strict, sense strongly suggests that active accretion is not happening in this case.

3.1.3. *Near-IR Quiescence*

Our original purpose for making simultaneous *CXO*/*HST* observations was to compare low-level near-IR and X-ray flux and spectral changes, with each observed with the same instrument, in order to look for correlations. Given that the near-IR source had faded considerably in the *HST* observations, rendering it only marginally detected in 2006, this was not possible. Compared to the handful of near-IR detections made throughout 2002-2003 (see Fig. 5) it is clear that 2005-2006 marked a period of near-IR quiescence in 1E 1048.1−5937. At the time of the 2005 *VLT* observations in which the AXP was faintly seen in K_S-band, its flux was consistent with the last detection in mid-2003. With *HST* in 2006 we find that its H and J magnitudes have dropped lower than ever before observed. There is marginal evidence for near-IR flux variability during quiescence on comparably short timescales to the variability in X-ray spectral parameters, although closely spaced near-IR monitoring observations are required to confirm this.

That the near-IR faded roughly in concert with the X-ray flux is notable, suggesting a correlation similar to that seen in AXP 1E 2259+586 (Tam et al. 2004). This is discussed further below. However such a correlation can be argued to be expected in both the magnetar and disk models. In the magnetar model it would imply that the near-IR emission is magnetospheric and hence varies, as do the X-rays, when the magnetospheric configuration varies (Heyl & Hernquist 2005; Beloborodov & Thompson 2007). In the disk model, a correlation between near-IR emission and X-ray flux is naturally expected since the putative disk is heated via X-ray illumination (Ertan et al. 2006; Wang et al. 2006), however why the torque should have varied strongly and non-simultaneously is a puzzle (see above).

In any case, the concurrence of the near-IR and X-ray quiescence and the timing stability is unlikely to be an accident. Similarly, the presence of the two flares and the subsequent strong torque changes are also not likely to be by chance.

3.2. *The 2007 March Event and its Aftermath*

1E 1048.1−5937 reactivated in 2007 March, when a sudden pulsed flux increase was observed (Fig. 1*c*), accompanied by a large spin-up glitch, the details of which will appear elsewhere (Dib et al., in preparation). Our follow-up X-ray observations with *CXO* and *Swift* show that the spectral parameters, pulse shape, total flux, and pulsed fraction are drastically changed since this flare occurred (Figs. 2 and 4). In particular, the total X-ray flux was >7 times greater in the 2−10 keV band compared with quiescence, while the pulsed fraction decreased from ∼75% to ∼20%. Compared to the previous long-term flares from 1E 1048.1−5937, the onset of this event took place more quickly by a factor of >4, the peak pulsed flux is ∼10% greater, and the "high" state appears to be lasting longer. Optical and near-IR follow-up with the *Magellan Telescope* and *VLT* (Wang et al. 2007; Israel et al. 2007) reveal an increase in both I and K_S-band of ∼1.3 mag. Very recently, Rea et al. (2007) reported on *XMM* ToO observations, and revealed that nearly three months after the flare onset, the total X-ray flux has decreased slightly but is still ∼5 times brighter than in quiescence.

3.2.1. *Near-IR Enhancement*

Previously, an anti-correlation between near-IR and X-ray flux in this AXP was suggested, based on the correspondence of the highest near-IR detection with a low point in X-ray pulsed flux[17] (Durant & van Kerkwijk 2005). Given the new measurements from both before and after the recent event, such an anti-correlation is highly questionable. The significant rise in near-IR flux

[17] Note that an error in Figure 4 of Durant & van Kerkwijk (2005) places the brightest K_S flux on the wrong date; we have corrected this in our Figure 5*c*.

now appears correlated with the most recent X-ray flare. Interestingly, in 2002, a high near-IR detection was *between* the two X-ray flares; this suggests that the near-IR emission is not exactly correlated with the X-rays, but rather an enhancement can precede, follow, or last longer than an X-ray enhancement. A near-IR brightening preceding an X-ray enhancement would rule out illuminated disk models for this source; frequent mid- or near-IR observations are required to check this. As discussed above, AXP 1E 2259+586 also demonstrated strongly correlated near-IR and X-ray flux decay following its large 2002 outburst (Tam et al. 2004), but in contrast, 4U 0142+61 was highly variable in the near-IR despite X-ray stability (Durant & van Kerkwijk 2006c), and has shown no evidence of near-IR changes coinciding with X-ray bursts (Gonzalez et al., in preparation). Note that the claim of correlated flux decay in the case of XTE J1810−197 (Rea et al. 2004) is under dispute (Camilo et al. 2007). Such inconsistent behaviour is puzzling for both the magnetar and disk models.

3.2.2. *Correlation between Pulsed Fraction and Total Flux*

One conclusion to be drawn from Figures 1*d* and 1*e* is that 1E 1048.1−5937's pulsed fraction $\mathcal{P}_\mathcal{F}$ is strongly anti-correlated with the total X-ray flux F_X, a trend already noticed by Tiengo et al. (2005) and Gavriil et al. (2006). Now, with our larger sample of data covering a wider dynamic range, we can quantify this correlation: we find a power-law dependence of $\mathcal{P}_\mathcal{F} \propto F_X^n$ where $n = -0.46 \pm 0.02$ (see Fig. 6), with F_X in the 2−10 keV range. In fitting, we set the index as a free parameter, ie. not tied to any model; therefore, some scatter is expected, as evident in the large $\chi^2_\nu = 9.36$ produced by the fit ($\nu = 14$ dof). However, in finding the uncertainty on n, we have scaled the $\mathcal{P}_\mathcal{F}$ data uncertainties to force $\chi^2_\nu = 1$, effectively scaling up σ_n as well. A similar correlation has been proposed in another AXP, 1RXS J170849.0−400910 (Dib et al. 2007a), although in that case it is such that the pulsed flux remains nearly constant in the presence of >50% total flux changes (Campana et al. 2007).

How could an increase in phase-averaged flux be met with a simultaneous decrease in pulsed fraction? A growing hot spot on the neutron-star surface, a result of either a changing magnitude or configuration of returning magnetospheric currents or internal processes, could at least in principle produce such an effect, if the initial hot spot size were large enough that its size as viewed from a distant observer were a significant fraction of the stellar surface. We note that Özel & Guver (2007) suggest that magnetar afterglows may be dominated by surface thermal, rather than magnetospheric, changes; detailed simulations of AXP pulsations using gravitational light bending and appropriate radiation beaming functions (e.g. Dedeo et al. 2001) in addition to magnetospheric scattering (Thompson et al. 2002; Fernández & Thompson 2007) are needed to see if the observed correlation can be reproduced.

3.2.3. *Correlation between Hardness and Total Flux*

A prediction made by the twisted magnetosphere model of Thompson et al. (2002) is that enhanced emission should also be spectrally harder, since both are associated with larger magnetospheric twist angles. Indeed, we observed a correlation between the total X-ray flux and spectral hardness: see Figure 6. Similar behaviour has also been reported in 1RXS J170849.0−400910 (Rea et al. 2005a; Campana et al. 2007). This can be interpreted as a confirmation of an important magnetar model prediction, namely that both the spectral hardness and the total flux should increase for an increasing magnetospheric twist angle (Thompson et al. 2002). Hardening of the spectrum might also be an expected effect of increased luminosity if a large injection of thermal seed photons is repeatedly up-scattered due to resonant cyclotron scattering feedback processes in the magnetosphere, thereby shifting the photon energies higher. Recently Özel & Guver (2007) have suggested that the hardness-intensity correlation in magnetars is a result of purely surface thermal changes, with no change in the magnetospheric configuration. It would be interesting to apply their model to the 1E 1048.1−5937 data as they span a much greater dynamic range in flux than did the sources studied by Özel & Guver (2007). This is beyond the scope of our paper, however.

3.2.4. *2007 Pulse Profile Changes*

As seen in the *CXO* data obtained after 2007 March, the pulse profile of 1E 1048.1−5937 changed abruptly after the X-ray flux enhancement and glitch. Several new harmonics are clearly visible, and are present in a largely energy-independent way (Fig. 4). This extra power in the higher harmonics clearly signals a complication of the surface and/or magnetospheric configuration. This change contrasts with that seen after the 2002 outburst of 1E 2259+586, which involved mainly an exchange of powers between the fundamental and first harmonic, with higher harmonics remaining relatively unchanged (Woods et al. 2004). Also, the change contrasts with that seen during the 1998 SGR 1900+14 giant flare, in which the SGR pulse profile simplified greatly immediately post-flare (Göğüş et al. 2002). However, the opposite occured followed the 2004 giant flare from SGR 1806−20 (Palmer et al. 2005), when a sinusoidal-to-complex evolution in pulse morphology took place, similar to that of 1E 1048.1−5937. This diversity of behaviors in magnetars post-outburst is problematic for understanding the underlying physics; indeed it indicates a wide variety of phenomenon phase space, which itself must be explained by models. The peculiar suppression of the 4th harmonic in the post-glitch 1E 1048.1−5937 profile is particularly puzzling to us; perhaps it indicates an important and unchangeable symmetry in the combined emission and viewing geometries, or perhaps it is a chance occurence and will not occur again in future events.

3.2.5. *2007 April Spectral Feature?*

In the *CXO* observation made on 2007 April 6, the one closest to and just after the 2007 March event, the X-ray spectrum of 1E 1048.1−5937 could not be well fit by a simple continuum model, in contrast with the other datasets. We identified a possible absorption line near 2.7 keV, though we note that the spectral model including this line is still not a good fit to the data. This suggests that other low-level features may be present as well, including a possible feature at

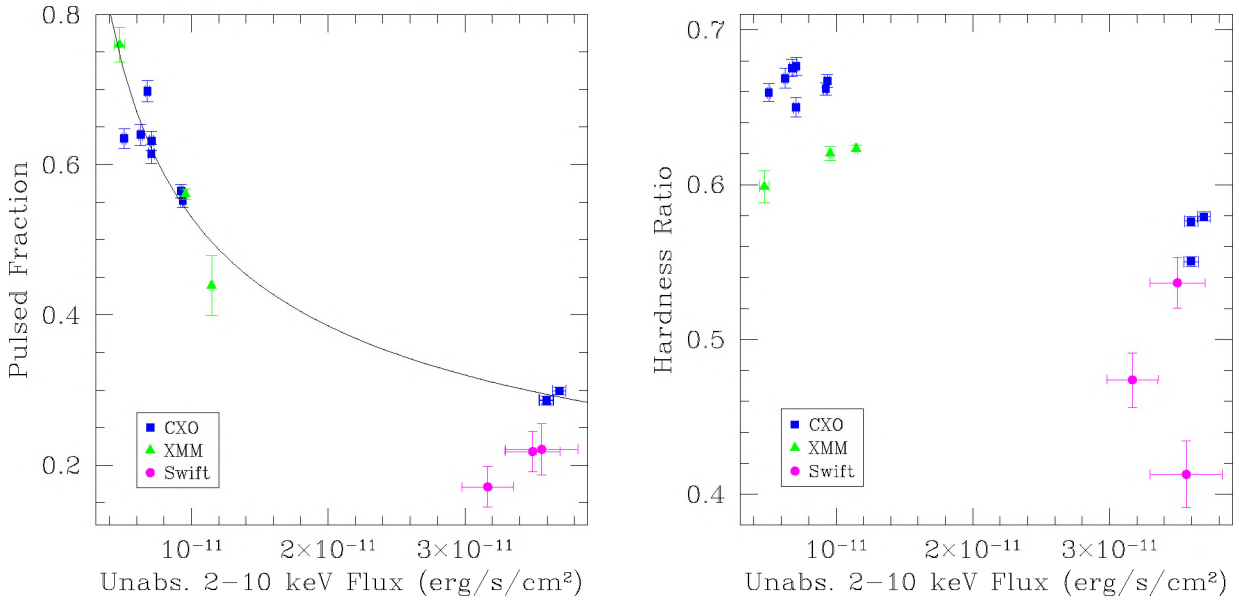

FIG. 6.— X-ray flux dependent properties of 1E 1048.1−5937, from 6 years of observations with *CXO* (*squares*), *XMM* (*triangles*), and *Swift* (*circles*). *Left:* Pulsed fraction vs. total unabsorbed flux, both in 2−10 keV. The solid black line shows the best-fit power law that describes the correlation between the two quantities. *Right:* Hardness ratio vs. total unabsorbed 2−10 keV flux. The hardness ratio is defined as $(S-H)/(S+H)$ where S and H are the phase-averaged count rates in the 1−3 and 3−10 keV bands, respectively.

roughly half the above line's energy, ∼1.3 keV. The putative 2.7 keV line joins the growing list of puzzling and sometimes statistically marginal AXP/SGR spectral features (Ibrahim et al. 2002, 2003; Rea et al. 2003, 2005a). Examples of some feature detections that are clearly statistically significant are, interestingly, repeatedly near ∼13 keV, e.g. in 1E 1048.1−5937 (Gavriil et al. 2002, 2006), in XTE J1810−197 (Woods et al. 2005), and very recently AXP 4U 0142+61 (Gavriil et al. 2007, and Gavriil et al., in preparation). The feature we see in the 2007 April data for 1E 1048.1−5937 are unlike any of these. It is perhaps more reminiscent of the absorption features seen in some "isolated neutron stars" (e.g. Bignami et al. 2003; van Kerkwijk et al. 2004), and, if similarly interpreted as an electron cyclotron line, implies a magnetic field of $\sim 3\times10^{11}$ G, or $\sim 6\times10^{14}$ G for a proton cyclotron line. The latter value is of course more in line with the field expected near the surface of a magnetar. However, the feature could also be an atomic transition (e.g. Mori & Ho 2007); it is difficult to know given the present data. Regardless, the spectrum 10 days later, on 2007 April 16, showed no such features, indicating that whatever their origin, it had subsided, and on a shorter timescale than that of any profile or flux relaxation.

3.2.6. *Comparison of the 2007 1E 1048.1−5937 Event with Other Similar Events*

The 2001-2002 flares observed in 1E 1048.1−5937 are unique in that they had very well resolved rise times of many weeks (GK04). The 2007 April event, by contrast, involved an X-ray pulsed flux enhancement that rose at least 4 times faster. In this sense it is perhaps more similar to the 2002 outburst of 1E 2259+586 (Kaspi et al. 2003), although in that case a brief rise could have been missed by the sparse monitoring. During that outburst, 1E 2259+586 exhibited an order-of-magnitude increase in pulsed and phase-averaged flux, as well as numerous other changes including (but not limited to) ∼80 SGR-like bursts. Similarly to 1E 1048.1−5937, both the total and pulsed flux increased during the 1E 2259+586 outburst, and the pulsed fraction decreased, going from 23% in quiescence down to 15% (Woods et al. 2004). However, the pulsed fraction was not as tightly correlated to the pulsed flux: the pulsed fraction recovered within ∼3 days (Zhu et al. 2007), whereas the flux took several months to return to its pre-outburst value (Woods et al. 2004). In terms of energetics, the total energy in 2−10 keV released in the 1E 2259+586 outburst was 3×10^{39} erg and 2×10^{40} erg during the rapid and gradual decay components, respectively (see Table 5 of Woods et al. 2004). For 1E 1048.1−5937, we estimate that up to 2007 April 28, the date of the last *CXO* observation, the total energy emitted is comparable, roughly 7×10^{39} erg (2−10 keV), based on the pulsed fraction-total flux correlation and assuming a distance of 2.7 kpc (Gaensler et al. 2005), or 8×10^{40} erg assuming 9.0 kpc (Durant & van Kerkwijk 2006a). Near-IR flux variability, possibly (in the case of 1E 1048.1−5937) and likely (in 1E 2259+586) correlated to X-ray flux, was observed following both events. That the 2007 1E 1048.1−5937 event clearly involved a large rotational glitch, as did the 2002 1E 2259+586 event, is also a commonality, although glitches at the time of the 2001-2002 flares could easily have been missed because of the large amount of timing noise and our inability to phase connect the data at that time (Dib et al., in preparation). SGR-like bursts from 1E 1048.1−5937 have not been observed thus far in 2007, but that does not preclude their existence given that our observing duty cycle is so low. Similar to 1E 1048.1−5937, 1E 2259+586 exhibited a pulse profile change, albeit one involving only the fundamental and first harmonic, in constrast to the appearance of higher harmonic structure in 1E 1048.1−5937. Finally, as in 1E 1048.1−5937, spectral hardening was observed during the 1E 2259+586 flare. Thus overall, the 2007 1E 1048.1−5937 event has practically all properties consistent with the 2002 1E 2259+586 event, but differs from

its earlier flares primarily by rise time.

The transient AXP XTE J1810−197 presents another interesting example for comparison. This AXP, which "turned-on" in late 2002 or early 2003 (Ibrahim et al. 2004), has been steadily declining in X-ray flux since, reaching apparent quiescence in 2005-2006 (Gotthelf & Halpern 2007). Unfortunately, very little is known about the onset of enhanced emission, ie., whether it was accompanied by a glitch/burst, or what the timescale of the rise was. While the exponential decay timescale of several years does resemble that of 1E 1048.1−5937's 2001-2002 post-flare behavior, how the most recent flare will fade is as yet undetermined. Furthermore, the peak and quiescent fluxes of XTE J1810−197 differed by a much greater amount, nearly 2 orders of magnitude (Gotthelf et al. 2004), while the recent total 2−10 keV flux increase in 1E 1048.1−5937 was by a factor of ∼7. Spectrally, XTE J1810−197 was harder in outburst and softer in quiescence, similar to 1E 1048.1−5937, when modelled as 2-temperature blackbody (Gotthelf & Halpern 2007) or as a blackbody plus power law (W. Zhu, private communication). One major distinction, however, is the clear evidence for a positive correlation between pulsed fraction and total flux in XTE J1810−197 (Gotthelf & Halpern 2007). While it may be tempting to link the transience of XTE J1810−197 to 1E 1048.1−5937-like post-flaring behaviour, the dissimilarities are important and remind us that we may be comparing mere coincidences.

Compared to the SGR giant flares, rare events in which an enormous amount of broad band energy (10^{44} – 10^{46} erg; Hurley et al. 2005) is output, the 1E 1048.1−5937 event is orders of magnitude less energetic. Giant flares release most of their energy in a short (<1 s), initial γ-ray spike, a property not observed in this event, although a small initial burst could have been missed. Furthermore, the 2007 event is prolonged, and while giant flares do gradually decay, the amount of energy in the tail is usually small compared to that of the spike (Woods et al. 2004; Hurley et al. 2005).

On the other hand, the gradual evolution of the persistent properties seen before and after the 2004 December giant flare of SGR 1806−20 do show some resemblance to 1E 1048.1−5937's behaviour. During this pre-flare period of enhanced burst activity in SGR 1806−20 that began in mid-2003, the pulsar torque, pulsed flux, total flux, and hardness increased on a ∼year timescale, peaking several months before the giant flare occurred in 2004 December, and continuing to decline well after the flare epoch (Woods et al. 2007). The gradual changes, particularly the well-resolved factor of >2 increase in total unabsorbed flux, perhaps resemble the 2001-2002 events of 1E 1048.1−5937 more than the 2007 event. As with 1E 1048.1−5937, a correlation was found between spectral hardness and intensity in SGR 1806−20, and there appeared to be some sort of physical connection between frequency derivative (or torque) evolution and variability in the spectrum and pulsed flux (Mereghetti et al. 2005; Woods et al. 2007). However, in SGR 1806−20, there was no evidence for a correlation between the phase-averaged flux, which likely peaked around 2004 October, and pulsed fraction, which was stable in the flux-enhanced pre-flare period but was lower than average in early 2005 when the persistent flux had approached quiescent levels (Rea et al. 2005b). Furthermore, SGR 1806−20's pulse profile was noticeably more sinusoidal while brightest (Woods et al. 2007), although the pulse profile likely changed as a direct results of the giant flare, rather than the slow evolution of persistent flux.

4. CONCLUSIONS

We have considered ∼10 yrs of multiwavelength observations of 1E 1048.1−5937. The source, in 2004-2006, gradually relaxed apparently back to quiescence in most respects, only to "awaken" suddenly in the glitch/flare event of 2007 March. By observing 1E 1048.1−5937 while quiescent, it has become apparent that previous instabilities in timing, X-ray and near-IR flux were likely all linked to the major long-term flaring events of 2001-2002, whose nature is yet unknown but likely includes changes in the stellar magnetosphere's current configuration. The asynchronous spin and X-ray flux variability we have observed is incompatible with expectations of the fossil disk accretion model. Following the most recent 2007 event, we observed total X-ray flux variability that is strongly correlated with X-ray pulsed fraction, X-ray spectral hardness, and changes in near-IR flux. These observations largely agree with expectations of the magnetar model. To date, the 1E 1048.1−5937 2007 event is ongoing, as is continued multiwavelength monitoring.

We thank Joe Hill and Lorella Angelini for their help with the *Swift* XRT data analysis, and Zhongxiang Wang for his help with the near-IR analysis. We thank the anonymous referee for many judicious comments that have improved the quality of the paper. FPG is supported by the NASA Postdoctoral Program administered by Oak Ridge Associated Universities at NASA Goddard Space Flight Center. PMW gratefully acknowledges support for this work from NASA/SAO through grant GO7-8077A. This research has made use of data obtained through the High Energy Astrophysics Science Archive Research Center Online Service, provided by the NASA/Goddard Space Flight Center, and is based on observations made with the NASA/ESA Hubble Space Telescope, obtained at the Space Telescope Science Institute, which is operated by the Association of Universities for Research in Astronomy, Inc., under NASA contract NAS 5-26555. These observations are associated with program #10761. This work has been supported by SAO grant GO7-8077Z, an NSERC Discovery Grant, the Canadian Institute for Advanced Research, and Le Fonds Québécois de la Recherche sur la Nature et les Technologies.

REFERENCES

Alpar, M. A. 2001, ApJ, 554, 1245
Anders, E. & Grevesse, N. 1989, Geochim. Cosmochim. Acta, 53, 197
Balucinska-Church, M. & McCammon, D. 1992, ApJ, 400, 699
Balucinska-Church, M. & McCammon, D. 1998, ApJ, 496, 1044
Beloborodov, A. M. & Thompson, C. 2007, ApJ, 657, 967
Bignami, G. F., Caraveo, P. A., De Luca, A., & Mereghetti, S. 2003, Nature, 423, 725

Camilo, F., Ransom, S. M., Halpern, J. P., Reynolds, J., Helfand, D. J., Zimmerman, N., & Sarkissian, J. 2006, Nature, 442, 892

Camilo, F., Ransom, S. M., Peñalver, J., Karastergiou, A., van Kerkwijk, M. H., Durant, M., Halpern, J. P., Reynolds, J., Thum, C., Helfand, D. J., Zimmerman, N., & Cognard, I. 2007, ApJ, 669, 561

Campana, S. & Israel, G. L. 2007, ATel, 1043

Campana, S., Rea, N., Israel, G. L., Turolla, R., & Zane, S. 2007, A&A, 463, 1047

Chatterjee, P., Hernquist, L., & Narayan, R. 2000, ApJ, 534, 373

Cox, A. N., ed. 2000, Allen's astrophysical quantities, 4th ed. (New York: AIP Press; Springer)

Dedeo, S., Psaltis, D., & Narayan, R. 2001, ApJ, 559, 346

Dib, R., Kaspi, V. M., & Gavriil, F. P. 2007a, ApJ, submitted (arXiv:0706.4156)

Dib, R., Kaspi, V. M., Gavriil, F. P., & Woods, P. M. 2007b, ATel, 1041

Duncan, R. C., & Thompson, C. 1992, ApJ, 392, L9

Durant, M. & van Kerkwijk, M. H. 2005, ApJ, 627, 376

—. 2006a, ApJ, 650, 1070

—. 2006b, ApJ, 650, 1082

—. 2006c, ApJ, 652, 576

Eichler, D., Gedalin, M., & Lyubarsky, Y. 2002, ApJ, 578, L121

Ekşı, K. Y. & Alpar, M. A. 2003, ApJ, 599, 450

Ertan, Ü. & Çalışkan, Ş. 2006, ApJ, 649, L87

Ertan, Ü., Göğüş, E., & Alpar, M. A. 2006, ApJ, 640, 435

Fernández, R. & Thompson, C. 2007, ApJ, 660, 615

Göğüş, E., Kouveliotou, C., Woods, P. M., Finger, M. H., & van der Klis, M. 2002, ApJ, 577, 929

Gaensler, B. M., McClure-Griffiths, N. M., Oey, M. S., Haverkorn, M., Dickey, J. M., & Green, A. J. 2005, ApJ, 620, L95

Gavriil, F. P., Dib, R., Kaspi, V. M., & Woods, P. M. 2007, ATel, 993

Gavriil, F. P. & Kaspi, V. M. 2004, ApJ, 609, L67, ; GK04

Gavriil, F. P., Kaspi, V. M., & Woods, P. M. 2002, Nature, 419, 142

—. 2004, ApJ, 607, 959

—. 2006, ApJ, 641, 418

Gotthelf, E. V. & Halpern, J. P. 2007, Ap&SS, 308, 79, (astro-ph/0608473)

Gotthelf, E. V., Halpern, J. P., Buxton, M., & Bailyn, C. 2004, ApJ, 605, 368

Heyl, J. S. & Hernquist, L. 2005, MNRAS, 362, 777

Hulleman, F., van Kerkwijk, M. H., Verbunt, F. W. M., & Kulkarni, S. R. 2000, A&A, 358, 605

Hurley, K., Boggs, S. E., Smith, D. M., Duncan, R. C., Lin, R., Zoglauer, A., Krucker, S., Hurford, G., Hudson, H., Wigger, C., Hajdas, W., Thompson, C., Mitrofanov, I., Sanin, A., Boynton, W., Fellows, C., von Kienlin, A., Lichti, G., Rau, A., & Cline, T. 2005, Nature, 434, 1098

Ibrahim, A. I., Markwardt, C. B., Swank, J. H., Ransom, S., Roberts, M., Kaspi, V., Woods, P. M., Safi-Harb, S., Balman, S., Parke, W. C., Kouveliotou, C., Hurley, K., & Cline, T. 2004, ApJ, 609, L21

Ibrahim, A. I., Safi-Harb, S., Swank, J. H., Parke, W., Zane, S., & Turolla, R. 2002, ApJ, 574, L51

Ibrahim, A. I., Swank, J. H., & Parke, W. 2003, ApJ, 584, L17

Israel, G. L., Campana, S., Testa, V., Mereghetti, S., Zane, S., Rea, N., Lo Curto, G., & Stella, L. 2007, ATel, 1077

Israel, G. L., Covino, S., Stella, L., Campana, S., Marconi, G., Mereghetti, S., Mignani, R., Negueruela, I., Oosterbroek, T., Parmar, A. N., Burderi, L., & Angelini, L. 2002, ApJ, 580, L143

Kaspi, V. M. 2007, Ap&SS, in press (astro-ph/0610304)

Kaspi, V. M., Chakrabarty, D., & Steinberger, J. 1999, ApJ, 525, L33

Kaspi, V. M., Gavriil, F. P., Chakrabarty, D., Lackey, J. R., & Muno, M. P. 2001, ApJ, 558, 253

Kaspi, V. M., Gavriil, F. P., Woods, P. M., Jensen, J. B., Roberts, M. S. E., & Chakrabarty, D. 2003, ApJ, 588, L93

Kuiper, L., Hermsen, W., den Hartog, P., & Collmar, W. 2006, ApJ, 645, 556

Marsden, D. & White, N. E. 2001, ApJ, 551, L155

Mereghetti, S., Tiengo, A., Esposito, P., Götz, D., Stella, L., Israel, G. L., Rea, N., Feroci, M., Turolla, R., & Zane, S. 2005, ApJ, 628, 938

Mereghetti, S., Tiengo, A., Stella, L., Israel, G. L., Rea, N., Zane, S., & Oosterbroek, T. 2004, ApJ, 608, 427

Mori, K. & Ho, W. C. G. 2007, MNRAS, 377, 905

Oosterbroek, T., Parmar, A. N., Mereghetti, S., & Israel, G. L. 1998, A&A, 334, 925

Özel, F. & Guver, T. 2007, ApJ, submitted (astro-ph/0612561)

Palmer, D. M., Barthelmy, S., Gehrels, N., Kippen, R. M., Cayton, T., Kouveliotou, C., Eichler, D., Wijers, R. A. M. J., Woods, P. M., Granot, J., Lyubarsky, Y. E., Ramirez-Ruiz, E., Barbier, L., Chester, M., Cummings, J., Fenimore, E. E., Finger, M. H., Gaensler, B. M., Hullinger, D., Krimm, H., Markwardt, C. B., Nousek, J. A., Parsons, A., Patel, S., Sakamoto, T., Sato, G., Suzuki, M., & Tueller, J. 2005, Nature, 434, 1107

Rea, N., Israel, G. L., Stella, L., Oosterbroek, T., Mereghetti, S., Angelini, L., Campana, S., & Covino, S. 2003, ApJ, 586, L65

Rea, N., Oosterbroek, T., Zane, S., Turolla, R., Méndez, M., Israel, G. L., Stella, L., & Haberl, F. 2005a, MNRAS, 361, 710

Rea, N., Testa, V., Israel, G. L., Mereghetti, S., Perna, R., Stella, L., Tiengo, A., Mangano, V., Oosterbroek, T., Mignani, R., Curto, G. L., Campana, S., & Covino, S. 2004, A&A, 425, L5

Rea, N., Tiengo, A., Israel, G. L., & Campana, C. 2007, ATel, 1121

Rea, N., Tiengo, A., Mereghetti, S., Israel, G. L., Zane, S., Turolla, R., & Stella, L. 2005b, ApJ, 627, L133

Stetson, P. B. 1987, PASP, 99, 191

Tam, C. R., Kaspi, V. M., van Kerkwijk, M. H., & Durant, M. 2004, ApJ, 617, L53

Thompson, C. & Duncan, R. C. 1995, MNRAS, 275, 255

Thompson, C. & Duncan, R. C. 1996, ApJ, 473, 322

Thompson, C., Lyutikov, M., & Kulkarni, S. R. 2002, ApJ, 574, 332

Tiengo, A., Mereghetti, S., Turolla, R., Zane, S., Rea, N., Stella, L., & Israel, G. L. 2005, A&A, 437, 997

van Kerkwijk, M. H., Kaplan, D. L., Durant, M., Kulkarni, S. R., & Paerels, F. 2004, ApJ, 608, 432, in press (astro-ph/0402418)

Wang, Z., Bassa, C., Kaspi, V. M., Bryant, J. J., & Morrell, N. 2007, ApJ, submitted (arXiv:0711.2290)

Wang, Z. & Chakrabarty, D. 2002, ApJ, 579, L33

Wang, Z., Chakrabarty, D., & Kaplan, D. L. 2006, Nature, 440, 772

Woods, P. M., Kouveliotou, C., Gavriil, F. P., Kaspi, V. M., Roberts, M. S. E., Ibrahim, A., Markwardt, C. B., Swank, J. H., & Finger, M. H. 2005, ApJ, 629, 985

Woods, P. M., Kaspi, V. M., Thompson, C., Gavriil, F. P., Marshall, H. L., Chakrabarty, D., Flanagan, K., Heyl, J., & Hernquist, L. 2004, ApJ, 605, 378

Woods, P. M., Kouveliotou, C., Finger, M. H., Göğüş, E., Wilson, C. A., Patel, S. K., Hurley, K., & Swank, J. H. 2007, ApJ, 654, 470

Woods, P. M. & Thompson, C. 2006, in Compact Stellar X-ray Sources, ed. W. H. G. Lewin & M. van der Klis (UK: Cambridge University Press)

Zhu, W., Kaspi, V. M., Woods, P. M., Gavriil, F. P., & Dib, R. 2007, ApJ, submitted (arXiv:0710.1896)